The lysine methyltransferase DOT1L controls CD4⁺ T cell differentiation and plasticity

Sebastian Scheer[1#], Michael Bramhall[1], Jessica Runting[1], Brendan Russ[1], Aidil Zaini[1], Jessie Ellemor[1], Grace Rodrigues[1], Judy Ng[1], Colby Zaph[1#]

[1]Infection and Immunity Program, Monash Biomedicine Discovery Institute, Department of Biochemistry and Molecular Biology, Monash University, Clayton VIC 3800, Australia.

[#]Correspondence:

colby.zaph@monash.edu, @colbyzaph ORCID ID: 0000-0002-9889-9848;

sebastian.scheer@monash.edu, @sebscheer, ORCID ID: 0000-0002-9716-5009

15 Innovation Walk, 3800 Clayton, VIC, Australia

SUMMARY

Histone methyltransferases comprise a major class of epigenetic enzymes that are emerging as important regulators of Th cell biology. Here, Scheer et al. report that DOT1L is a key regulator of the Th cell lineage and integrity, thereby affecting Th cell-dependent responses at mucosal sites.

ABSTRACT

$CD4^+$ T helper (Th) cell differentiation is controlled by lineage-specific expression of transcription factors and effector proteins, as well as silencing of lineage-promiscuous genes. Lysine methyltransferases (KMTs) comprise a major class of epigenetic enzymes that are emerging as important regulators of Th cell biology. Here, we show that the KMT DOT1L regulates Th cell function and lineage integrity. DOT1L-dependent dimethylation of lysine 79 of histone H3 (H3K79me2) is associated with lineage-specific gene expression. However, DOT1L-deficient Th cells overproduce IFN-γ under lineage-specific and lineage-promiscuous conditions. Consistent with the increased IFN-γ response, mice with a T cell-specific deletion of DOT1L are susceptible to infection with the helminth parasite *Trichuris muris* and resistant to the development of allergic lung inflammation. These results identify a central role for DOT1L in Th cell lineage commitment and stability, and suggest that inhibition of DOT1L may provide a novel therapeutic strategy to limit type 2 immune responses.

INTRODUCTION

Upon encounter of foreign antigens in the periphery, $CD4^+$ T helper (Th) cells can differentiate into several distinct cell lineages that have distinct physiological properties and functions. For example, Th1 cells are induced following viral or intracellular bacterial infection, produce the cytokine interferon-γ (IFN-γ) and activate macrophages to kill infectious organisms. In contrast, Th2 cells express interleukin (IL)-4, IL-5 and IL-13 following helminth infection and are required for immunity to this class of pathogens. These cells show a distinct and mutually exclusive cell fate, as the induction of the Th1 cell lineage program by the cytokine IL-12 and the transcription factor (TF) TBET leads to the production of IFN-γ, while repressing genes that characterise differentiated Th2 cells, such as IL-4 and IL-13 and the TF GATA3. Maintenance of lineage integrity is critical for optimal responses to a wide variety of pathogens.

Epigenetic modifiers, such as histone lysine methyltransferases (KMTs) have emerged as critical regulators of Th cell differentiation and function as their activity results in a defined state of chromatin, which enables the regulation of gene expression and in turn regulates cellular development and differentiation (He et al., 2013). We and others have previously shown that inhibition of KMTs has a profound impact on Th cell differentiation, lineage stability and function. For example, EZH2-dependent trimethylation of histone H3 at lysine 27 (H3K27me3) and SUV39H1/2-dependent H3K9me3 are important for lineage integrity of Th1 and Th2 cells (Tumes et al., 2013; Allan et al., 2012), while G9a-mediated H3K9me2 has been shown to control inducible regulatory T (iTreg) and Th17 cell differentiation (Lehnertz et al., 2010; Antignano et al., 2014). Importantly, KMTs are viable drug targets in a wide range of diseases (Schapira and Arrowsmith, 2016). Thus, a better understanding of the epigenetic mechanisms controlling Th cell differentiation and lineage stability could offer new strategies to modulate dysregulated Th cell function in disease.

Recently, in a screen using chemical probes targeting KMTs, H3K79 methyltransferase Disruptor of telomeric silencing 1-like (DOT1L) was shown to be an important regulator of Th1 cell differentiation in both murine and human Th cells (Scheer et al., 2019). DOT1L is the sole KMT for H3K79, performing mono-, di- and trimethylation in vivo (Min et al., 2003; Frederiks et al., 2008) since its knockout leads to a complete loss of H3K79 methylation (Jones et al., 2008). DOT1L-dependent H3K79 methylation has been suggested to directly promote transcriptional activation (Guenther et al., 2007; Steger et al., 2008). However, H3K79me2 has also been correlated to silenced expression (Zhang et al., 2006) and was further associated with both gene activation and repression in the same cell for separate genes (Chen et al., 2018). These

reports highlight the lack of clarity of H3K79 methylation in mammalian gene transcription, and the role of H3K79 methylation in Th cells has not been described in detail.

Here, we identify a key role for DOT1L in limiting the Th1 cell differentiation program in both Th1 and Th2 cells. The absence of DOT1L in Th cells leads to an impaired Th2 cell response in vivo during infection with the helminth parasite *Trichuris muris* or during allergic airway inflammation, identifying DOT1L as a potential therapeutic target to treat diseases associated with dysregulated Th2 cell responses at mucosal sites.

RESULTS AND DISCUSSION

To begin to understand the precise role of DOT1L and H3K79 methylation in Th cell differentiation, we generated a T cell-specific DOT1L-deficient mouse strain (DOT1L$^{\Delta T}$ mice) by crossing *Dot1l*$^{fl/fl}$ mice with *Cd4*-Cre transgenic mice (Fig. S1) and observed a specific reduction in DOT1L-dependent H3K79me2 levels within DOT1L-deficient T cells (Fig. 1 A). Consistent with our previous studies using the specific DOT1L inhibitor SGC0946 (Scheer et al., 2019), we found that loss of DOT1L resulted in heightened expression of IFN-γ under Th1 cell-polarising conditions. We also observed an increase in IL-13 production by Th2 cells, suggesting that DOT1L is critical for restraining lineage-specific gene expression. However, most striking was the production of IFN-γ by a significant proportion of cells stimulated under Th2 cell-inducing conditions (Fig. 1 B-D). The increased frequency of IFN-γ-producing cells was associated with reduced frequencies of GATA3-positive cells and a concomitant increase in TBET-positive cells (Fig. 1 E). Thus, DOT1L appears to be critically required for silencing of lineage-promiscuous expression of TBET and IFN-γ in Th cells. This increased IFN-γ production occurred rapidly after activation (Fig. 1 F), but was not due to increased proliferation (Fig. 1 G). Titration of αCD3 antibody demonstrated that loss of DOT1L rendered T cells hyper-sensitive to activating signals, with increased IFN-γ observed at all concentrations of αCD3 (Fig. 1 H). In addition, stimulation of freshly purified Th cells with phorbol ester and calcium ionophore (PMA/Iono) in the absence of direct T cell receptor stimulation further demonstrated that DOT1L is required to limit Th cell activation and IFN-γ production independently of the T cell receptor (Fig. 1 I). Importantly, when we sorted naive (CD44^{-} CD62L^{+}) Th cells from control or DOT1L-deficient mice, we found that DOT1L was still required to limit IFN-γ production (Fig. 1 J). Taken together, these results identify DOT1L as a cell-intrinsic regulator of Th cell lineage choice that is critical for limiting Th1 cell differentiation.

As we observed lineage-promiscuous expression of IFN-γ in the absence of DOT1L, we next tested whether DOT1L was required for lineage stability of Th cells (Tumes et al., 2013; Allan et al., 2012). We stimulated control or DOT1L-deficient Th cells under Th1- or Th2 cell-inducing conditions for three days, then washed and restimulated under opposing conditions for a further two days (Fig. 2 A). We found that the absence of DOT1L resulted in a loss of lineage integrity of both Th1 and Th2 cells. However, most striking was the loss of Th2 cell stability and the acquisition of IFN-γ production by a significant proportion of ex-Th2 cells, suggesting DOT1L is critical for silencing of Th1 cell lineage-specific genes in Th2 cells (Fig. 2 B). To directly test if

DOT1L was required to limit the Th1 cell differentiation program in *bona fide* Th2 cells or was more important in uncommitted activated Th cells in these cultures, we made use of IL-4/IL-13/IFN-γ triple reporter mice (IL-4-AmCyan; IL-13-dsRed; IFN-γ-YFP; CRY mice) mice to distinguish between committed Th1 (YFP^+) or Th2 ($AmCyan^+$ or $dsRed^+$) cells, or uncommitted but activated cells (Fig. 2 C). We activated Th cells from DOT1L-sufficient and -deficient CRY mice for three days under Th1- or Th2 cell-inducing conditions, sorted IFN-γ/YFP^+ (Th1) or IL-4/$AmCyan^+$ or IL-13/$dsRed^+$ (Th2) cells and restimulated under the opposing condition for two days. Committed Th1 and Th2 cells generated from DOT1L-sufficient mice were stable, with <4% of cells switching following reactivation. Interestingly, loss of DOT1L had no effect on the switching of committed Th1 cells, suggesting that DOT1L was dispensable for Th1 cell lineage stability. However, strikingly a significant frequency (>30%) of DOT1L-deficient Th2 cells stimulated under Th1 cell polarising conditions produced IFN-γ (Fig. 2 D), showing that DOT1L is critically required to maintain Th2 cells through the inhibition of IFN-γ production.

We next tested whether the increased early expression of IFN-γ in the absence of DOT1L leads to heightened IFN-γ expression through a feed-forward loop in Th cells. Treatment of WT Th1 cells with neutralising antibodies against IFN-γ (αIFN-γ) resulted in a significant reduction in expression of IFN-γ (Fig. 3 A, B). In contrast, IFN-γ expression was not reduced by αIFN-γ treatment in the absence of DOT1L, highlighting that expression of IFN-γ in the absence of DOT1L is independent of an IFN-γ feed-forward mechanism (Fig. 3 A, B). In line with this, DOT1L-deficient Th2 cells express IFN-γ despite being generated in the presence of αIFN-γ and in the absence of IL-12 (Fig. 3 C, D), identifying DOT1L as a critical cell-intrinsic regulator of the Th1 cell differentiation program. As αIFN-γ treatment failed to abolish IFN-γ production under both Th1- and Th2 cell-promoting conditions in the absence of DOT1L, we next analysed whether the transcription factor TBET was required for the expression of IFN-γ in these cells (Fig. 3 A, C). To do this, we made use of T cell-specific TBET and DOT1L/TBET double knockout mice ($TBET^{\Delta T}$ and DOT1L/$TBET^{\Delta T}$ mice). While TBET-deficient WT Th cells fail to differentiate into IFN-γ-producing Th1 cells, the absence of DOT1L allows for moderate IFN-γ expression in the absence of TBET (Fig. 3 A, B). Although the addition of αIFN-γ to the Th1 cell-promoting conditions had no effect in the absence of DOT1L, the combined deletion of DOT1L and TBET resulted in a further reduction in the frequency of IFN-γ-producing cells, suggesting that the increased frequency of IFN-γ-producing cells in DOT1L-deficient mice is dependent on the expression of TBET. Consistent with this finding, the lineage-promiscuous

expression of IFN-γ in Th2 cells was entirely dependent upon TBET, as DOT1L/TBET-deficient Th cells activated under Th2 cell-polarising conditions failed to produce any detectable levels of IFN-γ (Fig. 3 C, D). Thus, the dysregulated production of IFN-γ in Th1 and Th2 cells is TBET-dependent, suggesting that DOT1L deficiency affects the upstream Th1 cell lineage differentiation program rather than directly controlling IFN-γ expression.

Next, we made use of CRY mice to analyse the distribution of H3K79me2 in naive, or cultured and FACS-sorted *bona fide* Th1 or *bona fide* Th2 cells across the genome. Principal coordinate analysis (PCA) of three biological replicates showed high consistency within the samples of Th cell subsets and high diversity between groups (Fig. 4 A). H3K79me2 plot profiles of all genes ± 3 kb around the transcriptional start site (TSS) revealed increased coverage of H3K79me2 in all Th cell subsets around the TSS, consistent with a previous study (Wang et al., 2008). Levels of H3K79me2 were increased in Th1 and Th2 cells compared to naive Th cells, suggesting increased H3K79me2 coverage at genes in activated Th cells (Fig. 4 B). In general, H3K79me2 levels were high in all Th cell subsets at lineage-specific and low at non-Th lineage specific genes, such as for *Cd4* and *Myod1*, respectively. Increased coverage at the genes for *Ifng* and *Tbx21* in Th1, and *Il13* and *Gata3* in Th2 suggests that H3K79me2 is correlated with active, Th cell lineage-specific gene expression (Fig. 4C).

Our in vivo and ex vivo results using DOT1L$^{\Delta T}$ mice suggest that DOT1L is a negative regulator of the Th1 cell differentiation program. However, our results show that methylation of H3K79 by DOT1L is primarily associated with transcriptional activity (Fig. 4 C). We therefore performed genome-wide expression analysis by RNA-sequencing to understand the role of DOT1L-dependent H3K79me2 for specific gene expression in Th cells. PCA showed high similarities between the two biological replicates of each, naive Th, Th1 and Th2 samples from DOT1L$^{\Delta T}$ mice or *Cd4*-Cre^{+} controls (Fig. 4 D). Analysis of the number of up- and downregulated genes in Th cell subsets showed an increased number of genes with heightened levels in DOT1L-deficient Th cells (Fig. 4 E), identifying a potential inhibitory role for DOT1L in regulation of gene expression, despite the association of H3K79me2 with lineage-specific gene expression. MA-plots of significantly dysregulated genes (Th1/*Cd4*-Cre^{+} or Th2/*Cd4*-Cre^{+}; FDR cut-off 0.05, absolute log fold >0.585 ≃ >1.5-fold) in the absence of DOT1L show similar Th1 cell differentiation program-associated upregulated genes in Th1 and Th2 polarised cells (Fig. 4 F, G), which was partially already manifested in the unpolarised, naive state of the cells (Fig. 4 H).

As our data suggests a correlation of H3K79me2 coverage with gene expression, we clustered genes from each Th cell subset by gene expression into low (<20 counts), mid (~500 counts) or high (top 450 expressed genes) and assessed the presence of H3K79me2 ± 3 kb around the TSS. Analysis of the clusters revealed that strength of gene expression correlated to coverage for H3K79me2 with highly expressed genes showing highest average H3K79me2 coverage (Fig. 4 I) and little coverage for low expressed genes, which was independent of the Th cell subset (Fig. S2 A (Th1), Fig. 4 M (Th2)). However, our analysis also revealed the heterogeneity within the group of highly expressed genes with regard to H3K79me2 coverage at the TSS. Some highly expressed genes were highly enriched for H3K79me2 (subcluster “a”), while other highly expressed genes show little to no enrichment for H3K79me2 (subcluster “b”) (Fig. 4 J). This observation was less prominent in the clusters of intermediary expressed genes or in the cluster that showed low gene expression (Fig. S2B). We therefore analysed the genes in subclusters “a” and “b” for their expression in the absence of DOT1L. While genes in subcluster “a” showed a highly significantly reduced fold expression in the absence of DOT1L, genes in subcluster “b” showed a moderately reduced expression in the absence of DOT1L (Fig. 4 K), suggesting that DOT1L-dependent H3K79me2 is specifically required for maintaining the expression of a subset of highly expressed genes.

As we observed increased gene expression in the presence of H3K79me2 across the genome and a reduced Th1 cell differentiation program in the absence of DOT1L, we analysed whether the absence of DOT1L is associated with decreased expression of master regulators, such as TFs that inhibit the Th1 cell differentiation program. We found that 15 TFs were significantly downregulated across all Th cell subsets, seven of which are known to inhibit the Th1 cell differentiation program (red), five of which have not been defined with regard to their influence of the Th1 cell differentiation program (black) and three of which promote the Th1 cell differentiation program (green). Most prominently, the TFs BACH2, FOXP3 and NR4A3 were among the highest downregulated TFs across naive Th, Th1 and Th2 cells in the absence of DOT1L (Fig. 4 L), all of which have been correlated to limiting the Th1 cell differentiation program (Edwards et al., 2018; Yang et al., 2017; Sekiya et al., 2011). As an example, BACH2 was one of the highest downregulated TF that inhibits the Th1 cell differentiation program and clustered within the highest H3K79me2 coverage across all Th cell subsets (Fig. 7M, Fig. S2 C), suggesting a role of DOT1L and H3K79me2 in maintaining its gene expression across Th cell

subsets and thereby limiting the Th1 cell differentiation program. Thus, DOT1L controls Th cell differentiation through direct and indirect mechanisms.

Our results demonstrate that DOT1L is critical for limiting Th1 cell responses and maintaining Th2 cell lineage integrity in vitro. To test whether DOT1L is required for protective Th2 cell responses in vivo, we infected control DOT1L$^{FL/FL}$ or DOT1L$^{\Delta T}$ mice with the intestinal helminth parasite *Trichuris muris*. In this model, a high dose infection (~200 eggs) of WT mice results in the development of a protective Th2 cell-biased immune response, associated with goblet cell hyperplasia and mucus production, ultimately leading to worm expulsion. Following infection, DOT1L$^{\Delta T}$ mice maintained a significant worm burden at day 21 post-infection (Fig. 5 A, E), developed a non-protective Th1 cell response, with high levels of IFN-γ and low levels of IL-13 (Fig. 5 B, C), or produced low levels of *Trichuris*-specific IgG1 (Fig. 5 D). Further, treatment of mice with monoclonal antibodies against IFN-γ (αIFN-γ) failed to reduce the levels of IFN-γ and promote resistance to infection in the absence of DOT1L (Fig. 5 A-E). Thus, consistent with our in vitro results, DOT1L appears to be a T cell-intrinsic factor that is critical for limiting the development of Th1 cell responses.

Although protective in the context of helminth infection, Th2 cells are pathogenic in allergic inflammatory diseases such as asthma. To test if DOT1L deficiency prevented the development of pathogenic Th2 cells, we treated control DOT1L$^{FL/FL}$ or DOT1L$^{\Delta T}$ mice intranasally with house dust mite antigen (HDM). HDM induces a cascade of type 2 immune responses, including group 2 innate lymphoid cells, Th2 cells, and culminating with the recruitment and activation of eosinophils into the lungs. Consistent with our findings in vitro and during helminth infection, loss of DOT1L in T cells during allergic lung inflammation resulted in a significant increase in IFN-γ expression and reduced levels of IL-13 (Fig. 5 F). This reduced type 2 response led to significantly fewer eosinophils (CD45^{+} SiglecF^{+} CD11c^{neg}) in the lungs (Fig. 5 G). These results suggest that targeting DOT1L could provide a new therapeutic strategy to limit pathogenic Th2 cell responses.

In summary, the experiments described here provide the first evidence of a pivotal role for DOT1L and H3K79me2 in Th1/Th2 cell differentiation and lineage integrity, which has a significant impact on immunity to infection and the development of inflammation. These findings

place DOT1L as a central regulator of Th cell differentiation and identify this pathway as a potential therapeutic target to treat diseases associated with dysregulated Th cell responses.

FIGURE LEGENDS

Fig. 1. **DOT1L-deficient Th cells show increased production of IFN-γ.**

(A) Western blot analysis of histone extracts from sorted TCRb$^+$ CD4$^+$ (CD4), TCRb$^+$ CD8$^+$ (CD8) T cells and CD19$^+$ B cells (CD19) from control (DOT1L$^{FL/FL}$) or T cell conditional knockout mice for DOT1L (DOT1L$^{\Delta T}$) for H3K79me2 and pan-H3 (control). **(B)** Enriched Th cells from control (DOT1L$^{FL/FL}$) or DOT1L$^{\Delta T}$ mice under Th1 and Th2 polarising conditions. **(C)** Quantification of (B). **(D)** Quantitative PCR analysis of indicated genes of cells described in (B). **(E)** Signature Th1 and Th2 transcription factor analysis of the Th2 cells described in (A). **(F)** Kinetics of IFN-γ expression of enriched Th cells from control (DOT1L$^{FL/FL}$) or DOT1L$^{\Delta T}$ mice under Th1 polarising conditions. **(G)** Proliferative capacity of Th cells from control (DOT1L$^{FL/FL}$) or DOT1L$^{\Delta T}$ mice at indicated days after stimulation with plate bound αCD3 and αCD28 in the presence of IL-2. **(H)** Enriched peripheral Th cells from control (DOT1L$^{FL/FL}$) or DOT1L$^{\Delta T}$ mice were cultured for 4 days under Th1 polarising conditions at indicated concentrations of plate-bound αCD3. **(I)** Freshly isolated and 4 h phorbol ester and calcium ionophore-stimulated (PMA/Iono) peripheral Th cells from control (DOT1L$^{FL/FL}$) or DOT1L$^{\Delta T}$ mice in the absence of direct T cell receptor stimulation. **(J)** IFN-γ expression of sorted naive Th cells (CD44$^-$ CD62L$^+$) from control (DOT1L$^{FL/FL}$) or DOT1L$^{\Delta T}$ mice cultured for 3 days under Th1 polarising conditions. Error bars represent mean ± S.E.M. Data shown is representative of two (A,E-G,I,J) and three (B-D,H) independent experiments (n=3 mice per group). MFI: mean fluorescence intensity, CTR: CellTrace far red, RE: relative expression.

Fig. 2. **DOT1L maintains Th2 cell integrity.**

(A) Experimental setup of (B). **(B-D)** Enriched Th cells from control (DOT1L$^{FL/FL}$) or DOT1L$^{\Delta T}$ mice were cultured under Th1 or Th2 polarising conditions for 3 days and re-polarised under opposite conditions for an additional 2 days. **(B)** WT cells were cultured for 3 days, washed and re-polarised under opposite conditions for another 2 days. **(C)** Experimental setup using enriched Th cells from control (DOT1L$^{FL/FL}$-IL-4-AmCyan/IL-13-dsRed/IFN-γ-YFP (CRY)) or DOT1L$^{\Delta T}$-CRY mice in (D). **(D)** Th cells from indicated mice were cultured under Th1 or Th2 polarising conditions for 3 days, FACS-sorted for *bona fide* Th1 (YFP$^+$) or *bona fide* Th2 (AmCyan$^+$ and/or dsRed$^+$) cells and re-polarised under opposite conditions for 2 days. Error bars represent mean ± S.E.M. Data shown is representative of three (B) and two (D) independent experiments (B: n=3 mice per group; D: n=3 mice per group, pooled after sort).

Fig. 3. **Increased expression of IFN-γ in the absence of DOT1L is significantly reduced in the absence of αIFN-γ and TBET.**

(A,C) Ex vivo cultured Th cells from control (DOT1L$^{FL/FL}$), DOT1L$^{\Delta T}$, TBET$^{\Delta T}$ or DOT1L/TBET$^{\Delta T}$ mice under **(A)** Th1 or **(C)** Th2 polarising conditions in the absence (Th1) or presence (Th1+αIFN-γ, Th2) of neutralising antibodies against IFN-γ. **(B)** Quantification of (A). **(D)** Quantification of (C). Error bars represent mean ± S.E.M. Data shown is representative of two independent experiments (n=3 mice per group). ns: not significant.

Fig. 4. **DOT1L inhibits the Th1 cell differentiation program in Th cells via maintenance of H3K79me2.**

(A) Principal coordinates analysis (PCA) of H3K79me2 ChIP-sequencing from naive (CD62L^{+} CD44^{-}) Th, *bona fide* Th1 (IFN-γ^{+}) and *bona fide* Th2 (IL-4 and/or IL-13^{+}) cells from WT mice. **(B)** Analysis of H3K79me2 coverage ± 3 Kb around the TSS of all peak-called genes in naive Th, *bona fide* Th1 and *bona fide* Th2 cells. **(C)** H3K79me2 coverage at indicated genes. Data shown is from one H3K79me2 ChIP-seq experiment with three biological replicates and visualised with deepTools plotProfile or the Integrative Genomics Viewer (IGV). **(D)** PCA of RNA-sequencing from naive, *bona fide* Th1, and Th2 cells from control (Cre^{+}) and DOT1L$^{\Delta T}$ mice. **(E)** Number of up- and down-regulated genes from RNA-seq analysis (FDR cut-off 0.05, absolute log fold >0.585 ≃ >1.5-fold) of indicated cells. **(F-H)** MA-plots for *bona fide* Th1 (F), Th2 (G) and naive (H) Th cells. **(I)** Coverage of H3K79me2 ± 3 Kb around the TSS of genes in naive Th cells grouped by expression strength: low (<20 counts), mid (~500 counts), high (top 450 expressed genes). **(J)** Heatmap of H3K79me2 coverage ± 3 Kb around the TSS of highly expressed genes (Fig. 7 I: high). Subclusters “a” and “b” contain the top and bottom 1000 peaks (185 different genes for “a” and 143 different genes for “b”) regarding H3K79me2 coverage scores within the highly expressed genes. **(K)** Fold expression of genes in subcluster “a” and “b” (Fig. 7 J) in the presence or absence of DOT1L in naive Th cells. **(L)** Transcription factors (from RNA-seq experiment) that were downregulated across all Th cell subsets (naive Th, Th1, Th2) in the absence of DOT1L compared to control mice. Red indicates genes that inhibit the Th1 cell differentiation program, black shows unknown genes with regard to regulation of the Th1 cell differentiation program and green represents genes that are promoting the Th1 cell differentiation program. **(M)** Coverage of H3K79me2 ± 3 Kb around the TSS in Th2 cells grouped by expression strength: low (<20 counts), mid (~500 counts), high (top 450 expressed

genes) and the coverage of H3K79me2 for the TF BACH2. Data shown is representative of one experiment (n=2 for RNA-seq, n=3 for ChIP-seq).

Fig. 5. **DOT1L limits the development of Th1 cell responses during infection and inflammation in vivo.**

(A) Worm count in the cecum 21 days after the infection of control ($DOT1L^{FL/FL}$) or $DOT1L^{\Delta T}$ mice with 200 eggs of *Trichuris muris*. Where indicated, some $DOT1L^{\Delta T}$ mice were additionally treated with neutralising antibodies against IFN-γ. **(B)** Expression of IFN-γ and IL-13 from mesenteric lymph node cells (gated on viable $CD4^+$ T cells) 3 days post restimulation with αCD3 and αCD28 ex vivo. **(C)** Quantification of (B). **(D)** *Trichuris*-specific serum IgG1 from the same mice as (A). **(E)** Histology (PAS stain) of cecum tips from representative mice in (A). **(F)** QPCR analysis of whole lung tissue from mice sensitized and challenged with house dust mite allergen (HDM). **(G)** Eosinophils in the bronchoalveolar lavage from mice in (F). Data shown is representative of two independent experiments (n=4-5 mice per group).

METHODS

Mice

To create DOT1L$^{FL/FL}$ mice, we derived mice from DOT1L targeted ES cells (Dot1ltm1a(KOMP)Wtsi, KOMP ID:29070) and crossed them with FLP mice (Monash University). Subsequently, DOT1L$^{FL/FL}$ mice were crossed with CD4-Cre (C57BL/6 background) to generate DOT1L$^{\Delta T}$ mice (Supplementary Fig. 1). DOT1L$^{\Delta T}$ mice were crossed with IFN-γ-YFP reporter mice (Reinhardt et al., 2009) to create DOT1L$^{\Delta T}$IFN-γYFP mice. DOT1L$^{\Delta T}$CRY mice were generated by crossing DOT1L$^{\Delta T}$IFN-γYFP with 4C13R (Huang et al., 2015) mice. DOT1L/TBET$^{\Delta T}$ mice were created by crossing DOT1L$^{\Delta T}$ and TBET$^{\Delta T}$ (Intlekofer et al., 2008). Animals were maintained in a specific pathogen-free environment and used at 6-10 weeks of age and experiments were approved by the animal ethics committee of Monash University.

HDM model of allergic asthma

For the first 3 days of airway sensitization, mice were anesthetized under aerosolized isoflurane and intranasally instilled daily with 100 µg of house dust mite (HDM) antigen (Greer, Lenoir, NC) in 40 µl PBS. On days 13 to 17 post sensitization, mice were intranasally challenged daily with 25 µg of HDM antigen in 40 µl PBS before analysis on day 18. Bronchoalveolar lavage (BAL) was performed from the right lobes of the lung with three flushes of 800 µl PBS after clamping off the left lobe of the lung (used for histology and RNA isolation). BAL fluid and tissues were processed as previously described (Chenery et al., 2015). In short, cells from BAL were incubated with 200 µl FcBlock (1:500 rat serum, 20 µg/ml αCD16/32, clone 93) and stained with antibodies against SiglecF, CD11c, CD45 for the identification of eosinophils (SSC^{high}, SiglecF^{+}, CD11c^{-}, CD45^{+}). 123count eBeads were added prior to analysis for enumeration of cells.

Trichuris muris infection

Propagation of *Trichuris muris* eggs and infections were performed as previously described (Antignano et al., 2011). Mice were infected with 200 embryonated *T. muris* eggs by oral gavage to induce an intestinal infection over a period of 21 days. A subset of mice received 500 µg αIFN-γ (clone XMG1.2, BioXCell) in 200 µl PBS intraperitoneally at day 0, 4, 8, 12 and 16. Sacrificed mice were assessed for worm burdens by manually counting worms in the ceca using a dissecting microscope.

T cell assays

$CD4^+$ T cells were isolated from spleen and peripheral lymph nodes from indicated mice by negative selection using the EasySep™ Mouse $CD4^+$ T Cell Isolation Kit (StemCell Technologies Inc). 1.75 x 10^5 cells were cultured for 4 days in RPMI1640 supplemented with 10% heat-inactivated FCS, 2 mM L-glutamine, 100 U/ml penicillin, 100 µg/ml streptomycin, 25 mM HEPES, and 5 × 10^{-5} M 2-mercaptoethanol with 1 µg/ml each of plate-bound αCD3 (clone 145-2C11) and αCD28 (clone 37.51). Cells were cultured under Th0 (IL-2, 10 ng/ml), Th1 (IL-2 and IL-12, 10 ng/ml each; αIL-4 10 µg/ml).

Western blot

T cells ($CD4^+$ or $CD8^+$) and B cells ($CD19^+$) were sorted from the spleens of $DOT1L^{\Delta T}$ or CD4-Cre mice and pellets were frozen at -80˚C. Histones were extracted from frozen cell pellets by incubating in 0.2 N HCl overnight at 4˚C. Supernatants were run on 12% SDS-PAGE gels. H3K79me2 was detected using clone ab3594 (Abcam). A pan H3 antibody (ab1791, Abcam) was used as a loading control.

ELISA

T. muris-specific IgG1 was analysed as previously described. In short, ELISA plates were coated with o/n supernatant of adult worms, blocked with 10% NCS and serum was added in serial dilutions (1/20-1/2560). Secondary antibody (IgG1-HRP) was added at 1/1000 and incubated with 50 µl of TMB substrate until adequately developed. TMB substrate reaction was stopped by adding 50 µl of 1 N HCl and the plate was read at 450 nm.

Quantitative PCR

RNA from untreated lungs (clamped off during BAL) was isolated using 1 ml Trizol and mechanical disruption (one metal bead in a 2-ml-tube for 5 min and 60 Hz using the Qiagen TissueLyser LT) and chloroform extraction. CDNA was prepared using the High capacity cDNA reverse transcription kit (Applied Biosystems) according to the manufacturer's instructions. QPCR was performed using SYBR green and the following primers: *Ifng* forward 5′-GGATGCATTCATGAGTATTGCC-3′, reverse 5′-CCTTTTCCGCTTCCTGAGG-3′; *Il13* forward 5′-CCTGGCTCTTGCTTGCCTT-3′, reverse 5′- GGTCTTGTGTGATGTTGCTCA-3′; Actin b forward 5′-GGCTGTATTCCCCTCCATCG-3′, reverse 5′-CCAGTTGGTAACAATGCCATGT-3′.

RNA-sequencing

RNA was isolated from viable *bona fide* Th1 (YFP^+) or viable Th2 polarised cells of control ($CD4Cre^+$) and $DOT1L^{\Delta T}$ mice after 4 days of culturing under Th1 and Th2 polarising conditions, respectively, using the NucleoSpin RNA Kit from Macherey&Nagel according to the manufacturer's instructions and sequenced on a MiSeq paired-end run (75 x 75, v3; Illumina). Samples were aligned to the mm10 transcript reference using TopHat2, and differential expression was assessed using Cufflinks (Illumina). Visualization of the data was performed using DEGUST (https://github.com/drpowell/degust) and represent the average expression from 2 biological replicates. The RNA-Seq datasets described in this article are available at the National Center for Biotechnology Information (accession number GSE123966).

ChIP-qPCR and ChIP-sequencing preparation

1.5 x 10^6 sorted naive T cells ($CD4^+$ $CD44^-$ $CD62L^+$), *bona fide* Th1 (YFP^+) and *bona fide* Th2 (IL-4/IL-13^+) cells from control (CRY mice) or $DOT1L^{\Delta T}$-CRY mice were fixed for 8 min with 0.6% formaldehyde in 10 ml complete RPMI1640 media on an overhead rotator at room temperature. Fixing was stopped by adding 1 ml of 1.25 M glycine and incubating for 5 min on an overhead rotator at room temperature. Cells were pelleted at 600 x g for 5 min at 4˚C and washed twice with 10 ml ice cold PBS. Pellets were resuspended in 250 µl ChIP lysis buffer and stored at -80˚C. Cells were sonicated in 3 sets of 10 x 30 s ON, 30 s OFF at 4˚C using a Bioruptor (Diagenode) with intermittent quick vortex and centrifugation using polystyrene tubes. 200 µl of the supernatant was collected after centrifugation at 15,000 x g for 10 min at 4˚C and diluted in 800 µl ChIP dilution buffer containing 1:20 protease inhibitor. 40 µl of washed protein A and protein G magnetic beads (BioRad) and 2 µg of αH3K79me2 (ab3594) were added and incubated o/n at 4˚C on an overhead rotator. 20 µl of the supernatant (input) were diluted in 180 µl ChIP dilution buffer containing 0.3 M NaCl and incubated at 65˚C o/n for decrosslinking before using the PCR purification kit (Macherey&Nagel) for isolation of DNA. Next day, IP samples were washed consecutively twice with 1 ml of each ChIP low salt, ChIP high salt, ChIP LiCl and TE buffer using a magnet. Chromatin was eluted after the last wash by incubating twice with 150 µl ChIP elution buffer on an overhead rotator at room temperature. Both elutions were pooled and incubated at 65˚C o/n in the presence of 0.3 M NaCl. Next day, IP samples were purified using the PCR purification kit (Macherey&Nagel) and DNA was stored at -80˚C until QC and library preparation.

ChIP-sequencing

ChIP samples were processed using the MGITech MGIEasy DNA FS Library preparation kit V1 (according to the manufacturer's instructions: document revision A0) and sequenced using one lane of the MGISEQ-2000RS using an MGISEQ-2000RS High-Throughput Sequencing Set (PE100), yielding paired-end 100 base reads (according to the manufacturer's instructions: document revision A1). The ChIP-Seq datasets described in this article are available at the National Center for Biotechnology Information (accession number GSE138821).

Statistics

Statistical significance was determined by 2-tailed Student's t test or 2-way-ANOVA using GraphPad Prism 8 software (GraphPad Software, La Jolla, CA, USA). Results were considered statistically significant with $P \leq 0.05$. *: $p \leq 0.05$, **: $p \leq 0.01$, ***: $p \leq 0.001$.

ACKNOWLEDGEMENTS

We would like to thank Dr Kim Jacobson for constructive comments and advice on the manuscript. We thank the Monash animal facility, Micromon, the Monash flow core facility and the Monash bioinformatics core facility for their excellent technical support and assistance. We thank Dr Simon Phipps (QIMR Berghofer) for providing 4C13R mice (Huang et al., 2015). This work was supported by NHMRC Project grants (APP1104433 and APP1104466).

AUTHOR CONTRIBUTIONS

SS, CD and CZ designed the experiments.

SS, MB, JR, BR, JPN, QZ, AZ, JE, GR and JN performed experiments.

SS performed all mouse studies, ChIP-seq and RNA-seq experiments, in vitro assays and performed final ChIP-seq analysis.

SS and CZ wrote the manuscript.

REFERENCES

Allan, R.S., E. Zueva, F. Cammas, H.A. Schreiber, V. Masson, G.T. Belz, D. Roche, C. Maison, J.-P. Quivy, G. Almouzni, and S. Amigorena. 2012. An epigenetic silencing pathway controlling T helper 2 cell lineage commitment. *Nature*. 487:249–253.

Antignano, F., K. Burrows, M.R. Hughes, J.M. Han, K.J. Kron, N.M. Penrod, M.J. Oudhoff, S.K.H. Wang, P.H. Min, M.J. Gold, A.L. Chenery, M.J.S. Braam, T.C. Fung, F.M.V. Rossi, K.M. McNagny, C.H. Arrowsmith, M. Lupien, M.K. Levings, and C. Zaph. 2014. Methyltransferase G9A regulates T cell differentiation during murine intestinal inflammation. *J. Clin. Invest.* 124:1945–1955.

Antignano, F., S.C. Mullaly, K. Burrows, and C. Zaph. 2011. Trichuris muris infection: a model of type 2 immunity and inflammation in the gut. *J. Vis. Exp.*

Chenery, A.L., F. Antignano, K. Burrows, S. Scheer, G. Perona-Wright, and C. Zaph. 2015. Low-Dose Intestinal Trichuris muris Infection Alters the Lung Immune Microenvironment and Can Suppress Allergic Airway Inflammation. *Infect. Immun.* 84:491-501.

Chen, X., X. Liu, Y. Zhang, W. Huai, Q. Zhou, S. Xu, X. Chen, N. Li, and X. Cao. 2018. Methyltransferase Dot1l preferentially promotes innate IL-6 and IFN-β production by mediating H3K79me2/3 methylation in macrophages. *Cell. Mol. Immunol.* doi:10.1038/s41423-018-0170-4.

Edwards, C.L., M.M. de Oca, F. de Labastida Rivera, R. Kumar, S.S. Ng, Y. Wang, F.H. Amante, K. Kometani, T. Kurosaki, T. Sidwell, A. Kallies, and C.R. Engwerda. 2018. The Role of BACH2 in T Cells in Experimental Malaria Caused by Plasmodium chabaudi chabaudi AS. *Front. Immunol.* 9:2578.

Frederiks, F., M. Tzouros, G. Oudgenoeg, T. van Welsem, M. Fornerod, J. Krijgsveld, and F. van Leeuwen. 2008. Nonprocessive methylation by Dot1 leads to functional redundancy of histone H3K79 methylation states. *Nat. Struct. Mol. Biol.* 15:550–557.

Guenther, M.G., S.S. Levine, L.A. Boyer, R. Jaenisch, and R.A. Young. 2007. A chromatin landmark and transcription initiation at most promoters in human cells. *Cell*. 130:77–88.

He, S., Q. Tong, D.K. Bishop, and Y. Zhang. 2013. Histone methyltransferase and histone methylation in inflammatory T-cell responses. *Immunotherapy*. 5:989–1004.

Huang, Y., L. Guo, J. Qiu, X. Chen, J. Hu-Li, U. Siebenlist, P.R. Williamson, J.F. Urban Jr, and W.E. Paul. 2015. IL-25-responsive, lineage-negative KLRG1(hi) cells are multipotential "inflammatory" type 2 innate lymphoid cells. *Nat. Immunol.* 16:161–169.

Intlekofer, A.M., A. Banerjee, N. Takemoto, S.M. Gordon, C.S. Dejong, H. Shin, C.A. Hunter, E.J. Wherry, T. Lindsten, and S.L. Reiner. 2008. Anomalous type 17 response to viral infection by CD8+ T cells lacking T-bet and eomesodermin. *Science*. 321:408–411.

Jones, B., H. Su, A. Bhat, H. Lei, J. Bajko, S. Hevi, G.A. Baltus, S. Kadam, H. Zhai, R. Valdez, S. Gonzalo, Y. Zhang, E. Li, and T. Chen. 2008. The histone H3K79 methyltransferase Dot1L is essential for mammalian development and heterochromatin structure. *PLoS*

Genet. 4:e1000190.

Lehnertz, B., J.P. Northrop, F. Antignano, K. Burrows, S. Hadidi, S.C. Mullaly, F.M.V. Rossi, and C. Zaph. 2010. Activating and inhibitory functions for the histone lysine methyltransferase G9a in T helper cell differentiation and function. *J. Exp. Med.* 207:915–922.

Min, J., Q. Feng, Z. Li, Y. Zhang, and R.-M. Xu. 2003. Structure of the catalytic domain of human DOT1L, a non-SET domain nucleosomal histone methyltransferase. *Cell*. 112:711–723.

Reinhardt, R.L., H.-E. Liang, and R.M. Locksley. 2009. Cytokine-secreting follicular T cells shape the antibody repertoire. *Nat. Immunol.* 10:385–393.

Schapira, M., and C.H. Arrowsmith. 2016. Methyltransferase inhibitors for modulation of the epigenome and beyond. *Curr. Opin. Chem. Biol.* 33:81–87.

Scheer, S., S. Ackloo, T.S. Medina, M. Schapira, F. Li, J.A. Ward, A.M. Lewis, J.P. Northrop, P.L. Richardson, H.Ü. Kaniskan, Y. Shen, J. Liu, D. Smil, D. McLeod, C.A. Zepeda-Velazquez, M. Luo, J. Jin, D. Barsyte-Lovejoy, K.V.M. Huber, D.D. De Carvalho, M. Vedadi, C. Zaph, P.J. Brown, and C.H. Arrowsmith. 2019. A chemical biology toolbox to study protein methyltransferases and epigenetic signaling. *Nat. Commun.* 10:19.

Sekiya, T., I. Kashiwagi, N. Inoue, R. Morita, S. Hori, H. Waldmann, A.Y. Rudensky, H. Ichinose, D. Metzger, P. Chambon, and A. Yoshimura. 2011. The nuclear orphan receptor Nr4a2 induces Foxp3 and regulates differentiation of CD4+ T cells. *Nat. Commun.* 2:269.

Steger, D.J., M.I. Lefterova, L. Ying, A.J. Stonestrom, M. Schupp, D. Zhuo, A.L. Vakoc, J.-E. Kim, J. Chen, M.A. Lazar, G.A. Blobel, and C.R. Vakoc. 2008. DOT1L/KMT4 recruitment and H3K79 methylation are ubiquitously coupled with gene transcription in mammalian cells. *Mol. Cell. Biol.* 28:2825–2839.

Tumes, D.J., A. Onodera, A. Suzuki, K. Shinoda, Y. Endo, C. Iwamura, H. Hosokawa, H. Koseki, K. Tokoyoda, Y. Suzuki, S. Motohashi, and T. Nakayama. 2013. The polycomb protein Ezh2 regulates differentiation and plasticity of $CD4^+$ T helper type 1 and type 2 cells. *Immunity*. 39:819–832.

Wang, Z., C. Zang, J.A. Rosenfeld, D.E. Schones, A. Barski, S. Cuddapah, K. Cui, T.-Y. Roh, W. Peng, M.Q. Zhang, and K. Zhao. 2008. Combinatorial patterns of histone acetylations and methylations in the human genome. *Nat. Genet.* 40:897–903.

Yang, C., X.-R. Huang, E. Fung, H.-F. Liu, and H.-Y. Lan. 2017. The Regulatory T-cell Transcription Factor Foxp3 Protects against Crescentic Glomerulonephritis. *Sci. Rep.* 7:1481.

Zhang, W., X. Xia, D.I. Jalal, T. Kuncewicz, W. Xu, G.D. Lesage, and B.C. Kone. 2006. Aldosterone-sensitive repression of ENaCalpha transcription by a histone H3 lysine-79 methyltransferase. *Am. J. Physiol. Cell Physiol.* 290:C936–46.

Figure 1

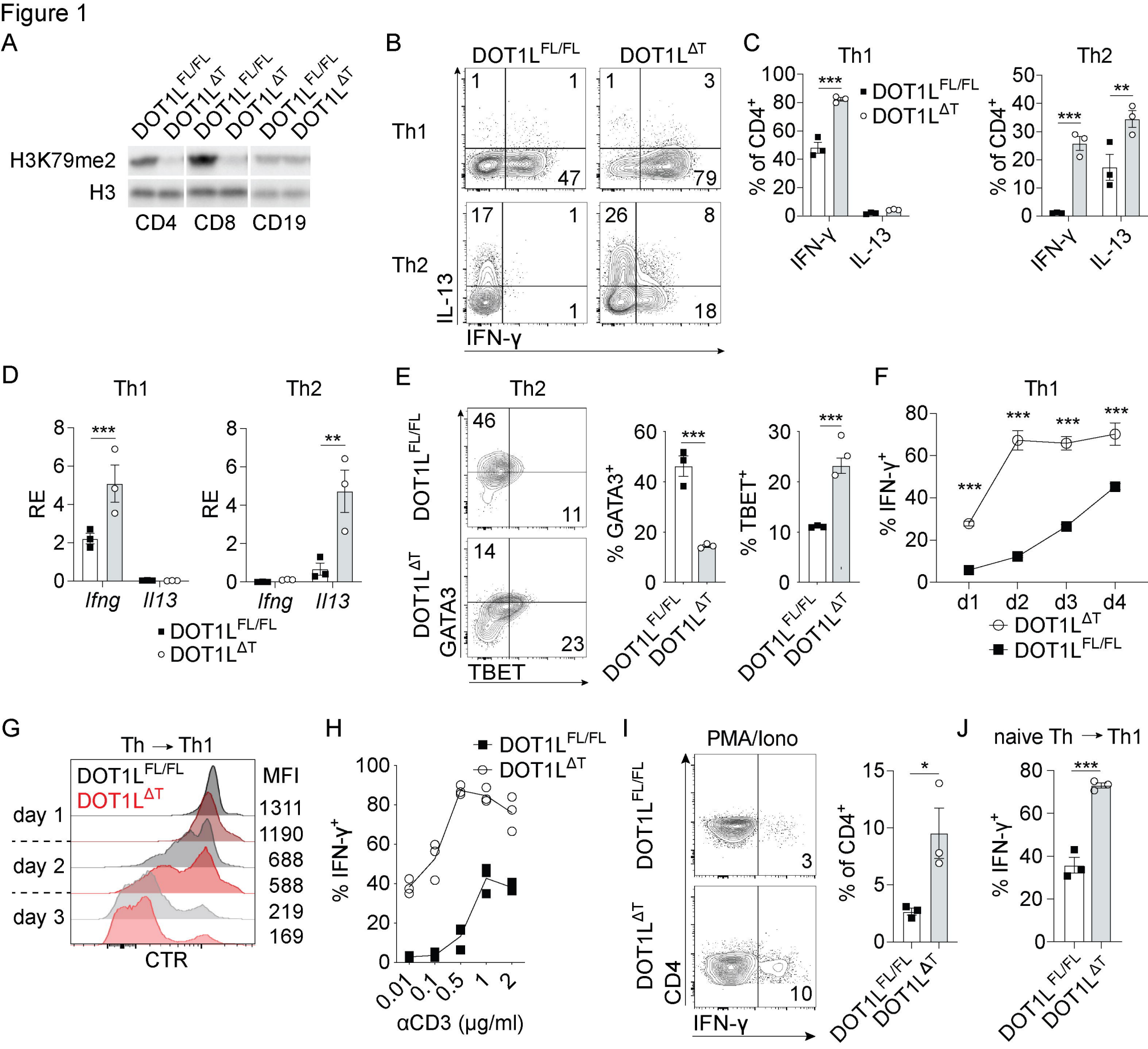
A
DOT1L FL/FL
DOT1L ΔT
H3K79me2
H3
CD4 CD8 CD19
B
DOT1L FL/FL
DOT1L ΔT
Th1
Th2
IL-13
IFN-γ
C
Th1
Th2
% of CD4+
DOT1L FL/FL
DOT1L ΔT
IFN-γ
IL-13
D
Th1
Th2
RE
Ifng
Il13
E
Th2
DOT1L FL/FL
DOT1L ΔT
GATA3
TBET
% GATA3+
% TBET+
F
Th1
% IFN-γ+
d1 d2 d3 d4
G
Th → Th1
MFI
day 1
day 2
day 3
CTR
H
% IFN-γ+
αCD3 (μg/ml)
I
PMA/Iono
CD4
IFN-γ
J
naive Th → Th1

Figure 2

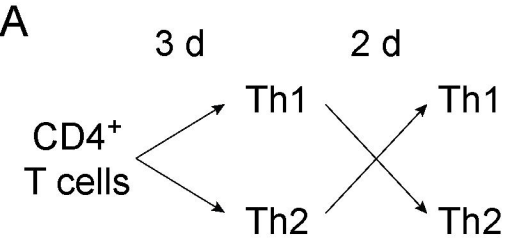
A
3 d
2 d
CD4+
T cells
Th1
Th2
Th1
Th2

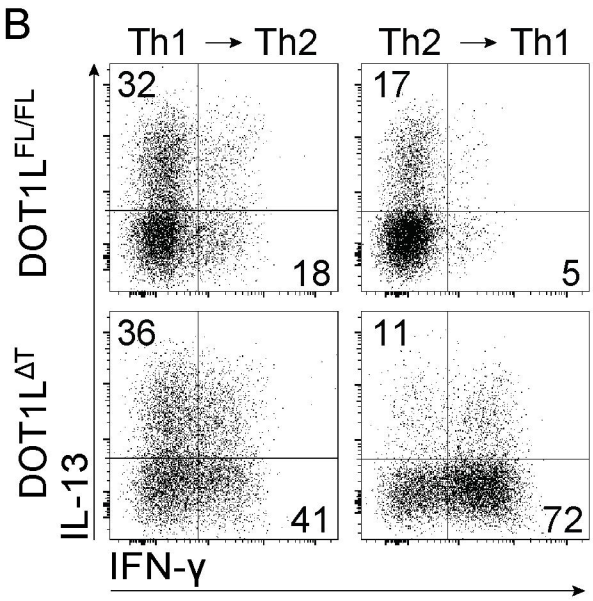
B
Th1 → Th2
Th2 → Th1
DOT1L FL/FL
DOT1L ΔT
32
18
17
5
36
41
11
72
IL-13
IFN-γ

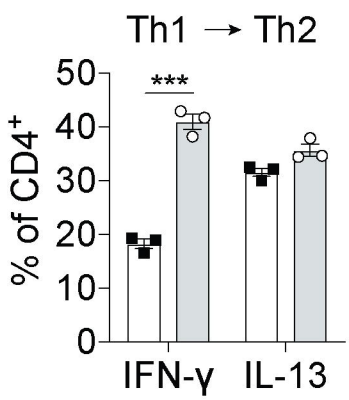
Th1 → Th2
% of CD4+
50
40
30
20
10
0
***
IFN-γ
IL-13

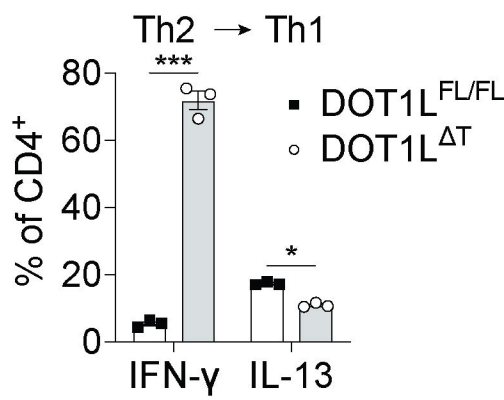
Th2 → Th1
% of CD4+
80
60
40
20
0
***
*
IFN-γ
IL-13
DOT1L FL/FL
DOT1L ΔT

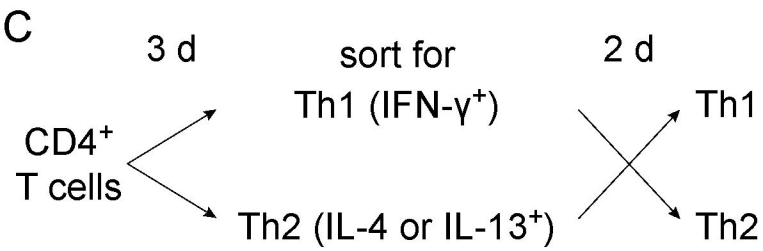
C
3 d
sort for
Th1 (IFN-γ+)
2 d
CD4+
T cells
Th2 (IL-4 or IL-13+)
Th1
Th2

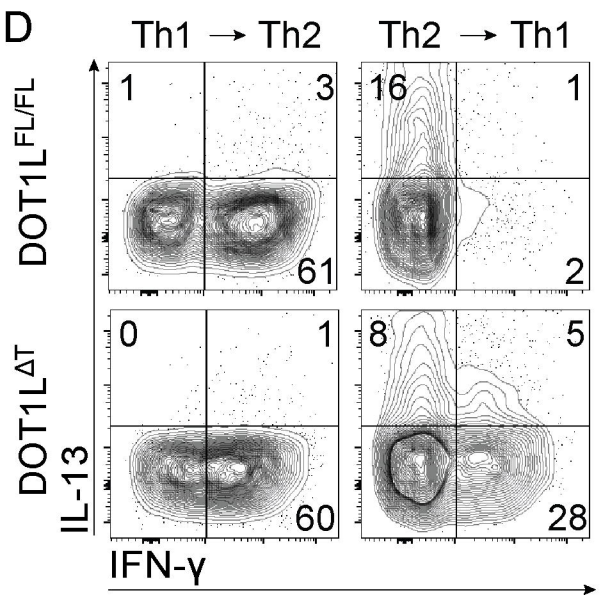
D
Th1 → Th2
Th2 → Th1
DOT1L FL/FL
DOT1L ΔT
1
3
61
16
1
2
0
1
60
8
5
28
IL-13
IFN-γ

Figure 3

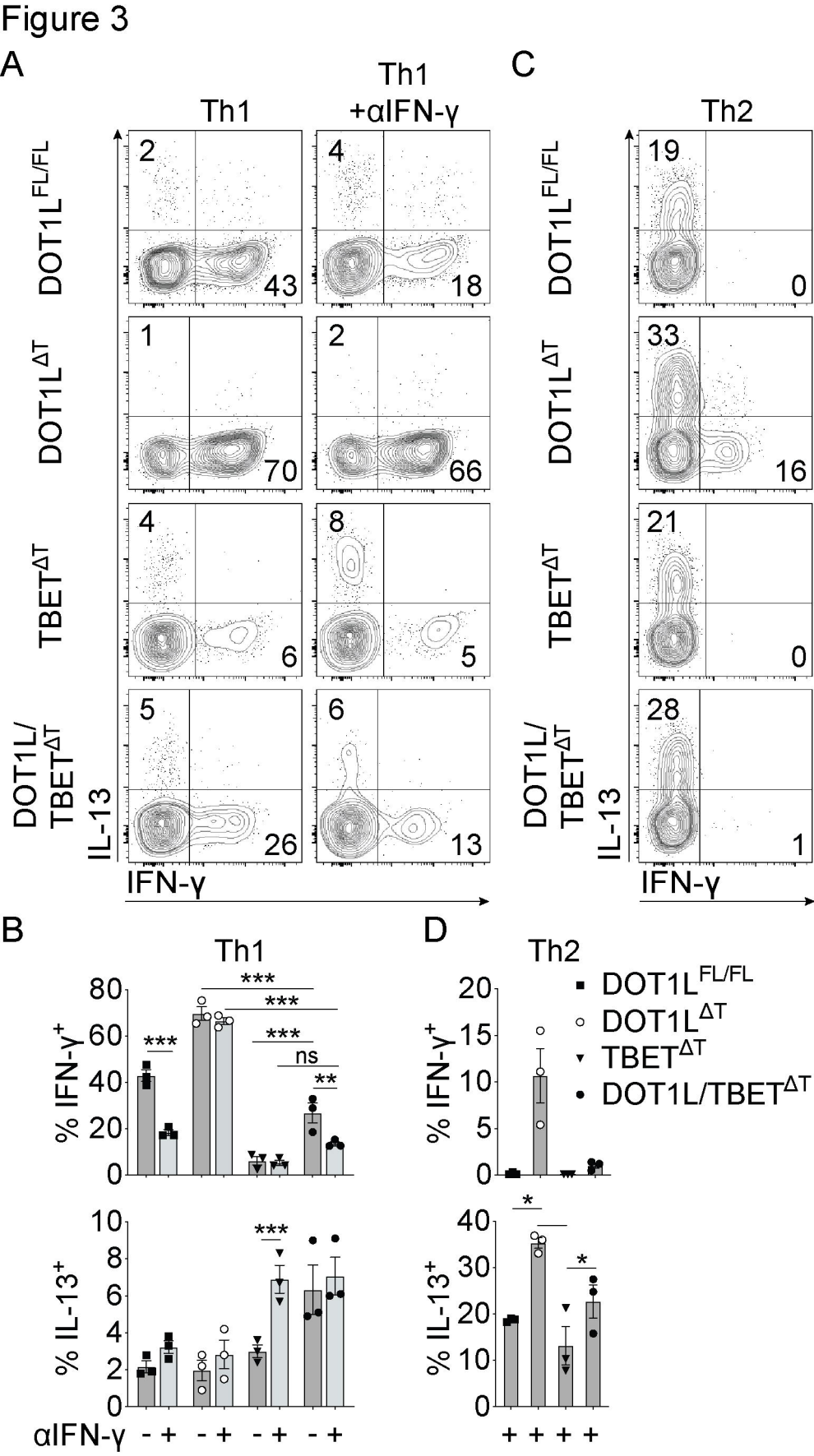
A
Th1
Th1 +αIFN-γ
C
Th2
DOT1L FL/FL
DOT1L ΔT
TBET ΔT
DOT1L/ TBET ΔT
2
43
4
18
19
0
1
70
2
66
33
16
4
6
8
5
21
0
5
26
6
13
28
1
IL-13
IFN-γ
B
Th1
D
Th2
% IFN-γ+
% IL-13+
***
ns
**
*
αIFN-γ - + - + - + - +
+ + + +
DOT1L FL/FL
DOT1L ΔT
TBET ΔT
DOT1L/TBET ΔT

Figure 4

Figure 5